Nanostructured Columnlike Tungsten Oxide Film by Anodizing Al/W/Ti Layers on Si

Alexander Mozalev,*,† Viacheslav Khatko,‡ Carla Bittencourt,§ Achim Walter Hassel,|| Gennadii Gorokh,† Eduard Llobet,‡ and Xavier Correig‡

Belarusian State University of Informatics and Radioelectronics, Brovki Str. 6, 220013 Minsk, Belarus, Universitat Rovira i Virgili, Av. Paisos Catalans 26, 43007 Tarragona, Spain, University of Mons-Hainaut, Parc Initialis, Avenue Nicolas Copernic 1, B-7000 Mons, Belgium, and Max-Planck-Institut für Eisenforschung, Max-Planck Str. 1, 40237 Düsseldorf, Germany

Received June 4, 2008. Revised Manuscript Received August 19, 2008

An Al/W/Ti trilayer sample prepared by a consecutive sputter deposition of titanium, tungsten, and aluminum layers onto a silicon wafer is first anodized in an oxalic-acid electrolyte at 27 V to convert the Al layer into nanoporous aluminum oxide. Further reanodizing the sample to 100 V results in the simultaneous growth of a 40 nm tungsten oxide layer beneath the alumina pores and discrete, columnlike regions of tungsten oxide (40 mn wide, 170 nm long, 30 nm apart) penetrating the alumina pores. The penetration of the alumina pores is assisted by the substantially increased transport number for tungsten species (0.48). The columnlike film derived after selective dissolution of the alumina matrix is mainly composed of amorphous WO_3 (with cation vacancies in the surface layer) and suboxides W_2O_5 and WO_2. Besides, Al_2O_3 and Si-, Ti-, and C-containing species are identified as minor components in the film. Annealing the film at 700−800 °C promotes the formation of polycrystalline phases of monoclinic WO_3 with *Pc* symmetry, monoclinic $WO_{2.72}$ with *P*2/*m* symmetry, and tetragonal WSi_2 with the body-centered lattice. The impact of these experimental findings on the detailed understanding of ionic transport processes determining the growth of the tungsten oxide nanostructures is considered.

Introduction

Anodic films on aluminum and other so-called valve metals (Ta, Nb, Ti, Zr, Mo, W, etc.) have been investigated for many years[1,2] as a result of their diverse practical applications[3] and, more generally, from the understanding that studying the anodic oxidation of these valve metals will give fundamental knowledge about the ionic transport processes determining oxide growth at ambient temperatures.[4] Within the field, there has been the interest in anodic oxidation of superimposed metallic layers, that is, a metal substrate covered with a thin layer of a different valve metal. The anodic oxidation of superimposed metal layers has first been analyzed theoretically by Pringle[5] and then experimentally confirmed by Shimizu and co-workers,[6−9] who pointed out that if the underlying metal forms an oxide of lower ionic resistivity than that of the outer metal oxide, randomly occurring "needles" of the inner metal oxide may penetrate into the layer of outer metal oxide. More recent works have revealed that in certain electrolytes for porous anodic alumina films, anodizing under appropriate conditions of a layer of Al deposited upon a layer of Ta, Nb, Ti, or Zr results in the formation of nanosized regions of the corresponding metal oxides due to systematic self-organization beneath the alumina pores.[10−13] Further, it was revealed that an additional reanodizing to a higher voltage of the initially anodized Al/Ta couple results in the directional growth of relatively long-aspect-ratio "nanocolumns" of tantalum anodic oxide.[12] These nanocolumns fill the pores lengthening proportionally to the applied voltage until dielectric breakdown interrupts their growth. The filling of pores was possible because of the high Pilling-Bedworth ratio (PBR) for Ta/Ta_2O_5 (2.5) and a high transport number for Ta^{5+} ions, ranging from 0.24[5] to 0.5.[12]

From the theoretical viewpoint, another potential candidate for the long-aspect-ratio nanocolumns that can be grown in the alumina pores is *tungsten* because of the high PBR for W/WO_3 (3.6)[5] and, more importantly, a high value for transport number of W^{6+} ions, which was reported to be

* Corresponding author. E-mail: sasha@nsys.by. Fax: +375 (17) 2932333.
† Belarusian State University of Informatics and Radioelectronics.
‡ Universitat Rovira i Virgili.
§ University of Mons-Hainaut.
|| Max-Planck-Institut für Eisenforschung.

(1) Vermilyea, D. A. *Acta Metall.* **1953**, *1*, 280.
(2) Schultze, J. W.; Lohrengel, M. M. *Electrochim. Acta* **1983**, *28*, 973.
(3) Lei, Y.; Cai, W.; Wilde, G. *Prog. Mater. Sci.* **2007**, *52*, 465.
(4) Thompson, G. E. *Thin Solid Films* **1997**, *29*, 192.
(5) Pringle, J. P. S. *Electrochim. Acta* **1980**, *25*, 1423.
(6) Shimizu, K.; Habazaki, H.; Skeldon, P.; Thompson, G. E.; Wood, G. C. *J. Surf. Finish. Soc. Jpn.* **1999**, *50*, 2.
(7) Skeldon, P.; Shimizu, K.; Thompson, G. E.; Wood, G. C. *Philos. Mag. B* **1990**, *61*, 927.
(8) Habazaki, H.; Skeldon, P.; Shimizu, K.; Thompson, G. E.; Wood, G. C. *Corros. Sci.* **1995**, *37*, 1497.
(9) Iglesias-Rubianes, L.; Skeldon, P.; Thompson, G. E.; Habazaki, H.; Shimizu, K. *J. Electrochem. Soc.* **2002**, *149*, B23.
(10) Mozalev, A.; Sakairi, M.; Saeki, I.; Takahashi, H. *Electrochim. Acta* **2003**, *48*, 3155.
(11) Tatarenko, N.; Mozalev, A. *Solid-State Electron.* **2001**, *45/6*, 1009.
(12) Mozalev, A.; Sakairi, M.; Takahashi, H. *J. Electrochem. Soc.* **2004**, *151*, F257.
(13) Mozalev, A.; Mozaleva, I.; Sakairi, M.; Takahashi, H. *Electrochim. Acta* **2005**, *50*, 5065.

10.1021/cm801481z CCC: $40.75
Published on Web 09/25/2008

0.30.[14] Therefore, it can be predicted that the electrochemical approach can help fabricate arrays of WO_3 nanocolumns, on semiconductor or dielectric substrates. Further thermal processing of the anodic tungsten oxide (TO) film is expected to enhance the semiconductor properties of the film due to full or partial crystallization of the amorphous oxide material. Single or polycrystalline WO_3 semiconductor films or wire arrays, prepared by various techniques including physical vapor deposition, sol−gel, pyrolysis, and pulsed laser deposition, exhibit excellent electrochromic, photocatalytic, and gas-sensing properties.[15,16] The functional properties of TO semiconductor may be significantly enhanced by lowering the feature size to the nanoscale,[17] by structuring film morphology using, for example, recently developed atmospheric-pressure chemical vapor deposition (APCVD) technique,[18,19] and by improving crystallographic texture of the film grains.[18−21] Therefore, the formation of nanostructured TO films has been among the active and competitive areas of research.

In the present work, tungsten oxide film with nanostructured columnlike surface morphology has been prepared by multistep anodic oxidation and high-temperature annealing of a thin layer of tungsten covered with an aluminum layer. Field emission scanning electron microscopy (SEM), X-ray photoelectron spectroscopy (XPS), time-of-flight secondary ion mass spectroscopy (ToF-SIMS), and X-ray diffraction (XRD) have been employed to analyze the morphology, chemical composition, and crystallographic structure of the anodically and thermally processed TO films. A model of nucleation and growth of the nanostructured tungsten oxide, involving the field-assisted ionic transport processes and relevant solid-state reactions, has been proposed and discussed here.

Experimental Section

Specimen Preparation. A single-crystal polished silicon wafer, of 76 mm in diameter, with (100) orientation and n-type conductivity (4.5 Ω cm), was used as a substrate. First, an adhesion titanium layer, about 20 nm thick, was sputter-deposited on the wafer. Then, a 350 nm thick tungsten layer and a 1000 nm thick aluminum layer were successively sputter-deposited onto the titanium layer. All metals were sputtered using a radio frequency (rf) magnetron method. The use of a silicon wafer was essential for providing a microscopically flat substrate surface to support the metal layers, for easy preparation of film fractures for SEM observations, and for avoiding ambiguity in interpreting later XPS, ToF-SIMS, and XRD results.

The wafer with the deposited Al/W/Ti layers was cut into pieces of 2 × 2 cm which were then individually anodized in a specially designed cylindrical two-electrode cell made of polytetrafluoroethylene (PTFE). The specimen was placed horizontally in the cell, and a PTFE ring was fastened tightly to the specimen so that only a surface area of 1.5 cm^2 was in contact with electrolyte. A Keithley 2410 programmed power supply controlled by LabVIEW software via PC and a general-purpose interface bus was used as the anodizing unit.

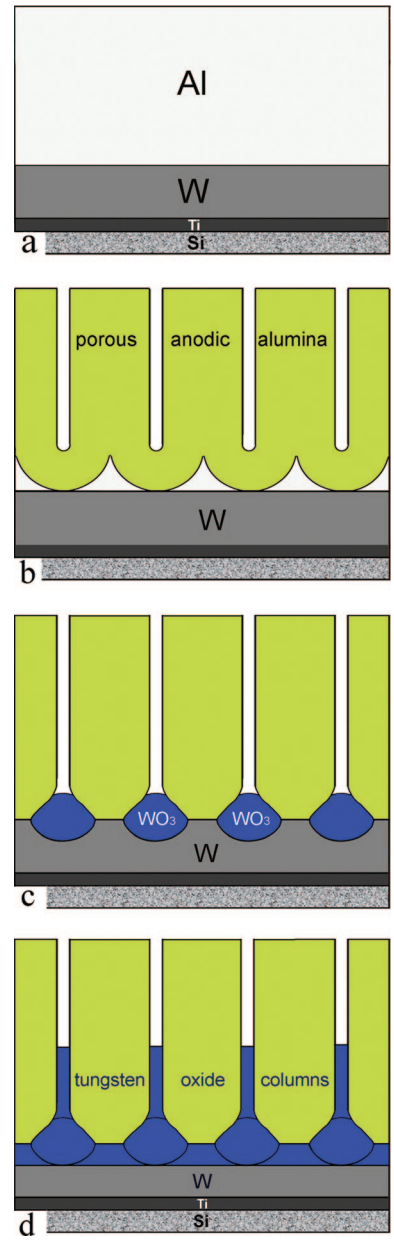

Figure 1. Main steps for forming nanostructured tungsten oxide film: (a) sputter-deposition of Al/W/Ti layers on Si, (b) porous anodizing the Al layer, (c) anodizing the W layer through the alumina pores, and (f) reanodizing the W layer to a higher voltage.

The process for forming nanostructured TO films is shown schematically in Figure 1. First, the Al layer is electrochemically converted into aluminum oxide with self-organized nanoporous morphology[4] (Figure 1a). Once the scalloped alumina barrier layer reaches the W layer, discrete nanosized regions of tungsten oxide are raised from the tungsten metal locally penetrating the alumina barrier layer beneath the alumina pores[10] (Figure 1b). Following anodizing, the specimen is reanodized to a more anodic voltage in an aqueous electrolyte for compact-type anodic film formation. It is expected that during reanodizing the discrete regions will continue to grow in size gradually filling the pores and getting a shape of

(14) Davies, J. A.; Domeij, B.; Pringle, J. P. S.; Brown, F. *J. Electrochem. Soc.* **1965**, *112*, 675.
(15) Tsirlina, G. A.; Miecznikowski, K.; Kulesza, P. J.; Borzenko, M. I.; Gavrilov, A. N.; Plyasova, L. M.; Molina, I. Y. *Solid State Ionics* **2005**, *176*, 1681.
(16) Ponzoni, A.; Comini, E.; Ferroni, M.; Sberveglieri, G. *Thin Solid Films* **2005**, *490*, 81.
(17) Hassel, A. W.; Smith, A. J.; Milenkovic, S. *Electrochim. Acta* **2006**, *52*, 1799.
(18) Blackman, C. S.; Parkin, I. P. *Chem. Mater.* **2005**, *17*, 1583.
(19) Ashraf, S.; Blackman, C. S.; Binions, R.; Parkin, I. P. *Polyhedron* **2008**, *26*, 1493.
(20) Korotcenkov, G. *Sens. Actuators, B* **2005**, *107*, 209.
(21) Khatko, V.; Mozalev, A.; Gorokh, G.; Solovei, D.; Guirado, F.; Llobet, E.; Correig, X. *J. Electrochem. Soc.* **2008**, *155*, K116.

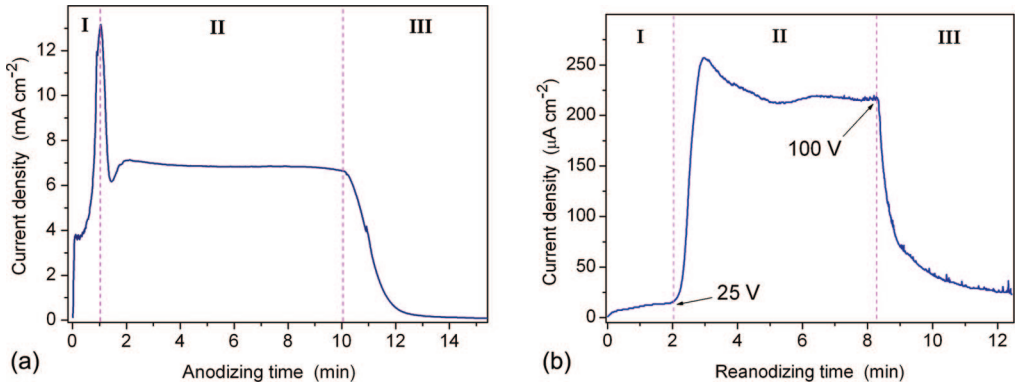

Figure 2. Current−time responses for (a) anodizing and (b) reanodizing of an Al/W/Ti/Si sample. Anodizing was done in 0.9 M $H_2C_2O_4$ by sweeping the voltage to 27 V (part I) followed by constant voltage polarization (II and III). Reanodizing was done in 0.5 M H_3BO_3 by voltage sweep from 0 to 100 V (I and II), followed by constant voltage polarization (III).

columns or rods, in the manner described in previous work.[12] At the film/metal interface, growing oxide nanocolumns may merge to form a continuous oxide layer under the columns (Figure 1c). After reanodizing, the specimen is solution heat-treated to selectively dissolve the alumina and expose the columnlike TO anodic film for further analysis. In order to crystallize the amorphous TO film, the specimen is to be annealed at temperatures above 300−400 °C.[21]

Specimen Characterization. The surfaces and cross fractures of specimens were observed in a LEO 1550 VP electron microscope (Leo Elektronenmikroskopie GmbH, Oberkochen, Germany) operated at 20 kV and in a JSM 6400 electron microscope (JEOL Ltd., Japan) operated at 30 kV. The chemical composition and bonding states in the anodic films were examined by XPS analysis carried out in a VG-ESCALAB 220iXL instrument equipped with an Al Kα monochromatized X-ray beam. The X-ray emission energy was 25 W with a 15 kV accelerating voltage focused to a spot of 250 × 1000 μm. Typical operating pressures were better than 10^{-9} Torr. The emitted electrons were detected by a hemispherical analyzer at fixed pass energies of 50 eV for the survey spectra and 20 eV for the high-resolution spectra. The takeoff angle was 90° (the angle between the sample surface and the direction of photoelectrons to the detector). For the depth-profiling analysis, selected specimens were sputtered using an argon ion beam of 1 kV provided by a standard ion gun with a filament emission current of 1 μA and a spot size of 2 × 2 mm. The angle of incidence of the sputtering beam was 55° with respect to the substrate surface. After each sputter cycle (15 s), the XPS data were collected. The spectra analysis was performed with The Advantage data processing software.

The profiling analysis of anodic films was complemented by ToF-SIMS performed with an ION-TOF IV instrument (ION-TOF GmbH, Münster, Germany) with the depth profiles measured using the instrument in dual beam mode. A 15 keV Ga^+ ion beam of a current of 1.56 pA, rastered over a scan area of 100 × 100 μm, was used as the analysis beam. The sputtering was performed using a 2 keV Cs^+ ion beam at a current of 69.8 nA, rastered over an area of 300 × 300 μm. Both ion beams were directed under an angle of 45° with respect to the surface normal and were aligned in such a way that the analyzed ions were taken from the middle of the sputtered crater. The detection was made in the positive and negative ion modes. For each spectrum the mass scale was calibrated by using well-identified ions for the positive and negative spectra.

The crystal structure of the anodized and annealed Al/W/Ti/Si samples was determined by XRD in a Siemens D5000 diffractometer (BRUKER AXS Inc., U.S.A.) having Bragg−Brentano parafocusing geometry and vertical $\theta-\theta$ goniometer and equipped with a grazing incidence ($\omega = 1.7°$) attachment with a scintillation counter as the detector. The data were collected with an angular step of 0.05° at 5 s per step. Annealing of samples was carried out in an Anton-Paar HTK10 high-temperature chamber with a platinum ribbon as a heating stage. The patterns were collected at ΔT = 100 °C after 300 s of delay time at a heating/cooling rate of 0.17 °C s^{-1}. The temperature range used for the analysis was set to 23−800 °C. Either a static air or a nitrogen gas (after the chamber was pumped down to 10^{-2} mbar) was introduced in the chamber throughout the measurements. Cu Kα radiation was obtained from a copper X-ray tube operated at 40 kV and 30 mA.

Results

Anodizing Behavior. The electrical and electrolytic conditions employed here for anodic processing of the aluminum layer have been selected to obtain a high-quality porous anodic film of desired thickness, pore structure, and chemical composition.[12] It is well-known that in oxalic acid-based electrolytes anodic oxide growth proceeds at relatively low anodizing voltages, down to 25 V, but rather high current densities, up to 500 mA cm^{-2}, which are known to be the best conditions for pore self-organization in the anodic alumina films.[3,22] Further, as the voltage determines the size of the oxide cells, the pore population density could be as high as 10^{11} cm^{-2} while the mean pore diameter could be scaled down to about 10−15 nm.[23] Importantly, both parameters are not expected to change across the film of several micrometers thickness because the aggressiveness of the electrolyte is weak at room temperature. With reference to previously reported results on anodizing various metal couples including aluminum,[10−13] it is expected that, with the above-mentioned pore size, pore density, and overall film thickness, the anodic alumina film grown in the Al/W couple will be an appropriate host for later formation of tungsten oxide nanocolumns in the alumina pores.

Figure 2a shows the current−time response for the potentiodynamic polarization of the Al/W/Ti/Si sample in 0.9 M $H_2C_2O_4$ electrolyte by sweeping the voltage at 0.5 V s^{-1} from zero to 27 V and then stabilizing this voltage over

(22) Surganov, V.; Mozalev, A.; Mozaleva, I. *Russ. J. Appl. Chem.* **1995**, *68*, 1638.
(23) Ono, S.; Masuko, N. *Surf. Coat. Technol.* **2003**, *169−170*, 139.

a period of time. At the commencement of the voltage sweep, the anodizing current rises sharply, with a short retarding period preceding the initiation of pores, reaching eventually about 13 mA cm^{-2} when the voltage attains 27 V (part I, Figure 2a). At this moment, the voltage sweep is stopped and after a short transient period the current takes up a relatively steady-state value, of about 7 mA cm^{-2} (part II). During part II, a porous alumina film steadily grows down to the W layer, with a rate proportional to the current density. Once the film/metal interface reaches the W layer, the current begins to decay (the end of part II). The current is allowed to decrease until it drops at least 10-fold from the steady-state value (part III, Figure 2a). The above procedure is further referred to as anodizing.

Figure 2b shows the current−time curve for the potentiodynamic reanodization of the initially anodized Al/W/Ti/Si sample by sweeping the voltage in 0.5 M H_3BO_3 at a constant rate of 0.2 V s^{-1} from 0 to a selected value and then stabilizing this voltage value over a period of time. From the figure, no hints on an ionic current flow through the film at the commencement of voltage sweep are found, because of the presence of a potential barrier, which is the local areas of tungsten oxide separating the metal from the electrolyte (part I, Figure 2b). Only when the voltage is raised to about 25 V does the measured current begin to rise, due to restoring the ionic conduction[24] throughout the TO areas. Soon beyond 35 V, the current attains a relatively steady value of about 220 μA cm^{-2} (part II). The voltage sweep is stopped at 100 V, this followed by current decay over about 5 min (part III, Figure 2b). Noteworthy is that during the reanodizing it was possible to raise the voltage up to above 200 V, but voltage fluctuations occurred above 120−130 V. This was due to the combined effects of stress generation during the penetration of growing tungsten oxide into alumina pores and poor adhesion on physical defects between the metal layers. The steady-state current behavior during the voltage sweep (part II, Figure 2b) followed by the smooth current decay during the constant-voltage polarization confirms the growth of solid-state anodic oxide on the tungsten layer.

SEM Observation. Figure 3 shows SEM views of the Al/W/Ti/Si sample after anodizing followed by reanodizing as described in the Experimental Section. From Figure 3a, the rf-magnetron-sputtered Al film was polycrystalline with grains of about 400 nm in average. The grain size appeared to be substantially smaller than in the case of an aluminum film grown by a direct-current magnetron method.[25] The outlets of pores are clearly seen on the former grain faces and along the grain boundaries (Figure 3b). During anodizing, grain boundaries are generally preferred sites for dissolution and nucleation of pores because they are inherently more active than the adjacent grain matrix. The smaller grains and their relatively close packaging in the film seem to be advantageous for improving the pore regularity already at the film surface.

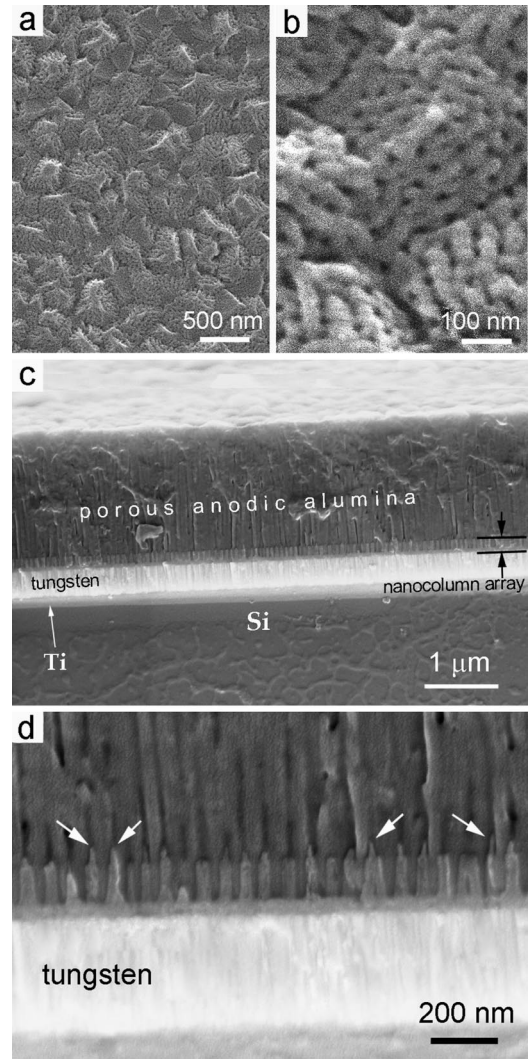

Figure 3. SEM views of (a, b) the surface and (c, d) cross fractures of the Al/W/Ti/Si sample after anodizing followed by reanodizing as shown in Figure 2.

Figure 3c,d represents SEM images of a cross fracture of the Al/W/Ti/Si sample after anodizing at 27 V followed by reanodizing to 100 V. A layer of porous alumina is observed at the upper half of the micrograph of Figure 3c. The residual (unanodized) tungsten layer is identified as the wide light band (Figure 3c,d). The residual tungsten is relatively uniform in thickness, with mainly polycrystalline rod-like grains that are typically developed by the magnetron method.[9] Between the W layer and Si substrate, an additional band is observed, which is associated with the Ti underlayer. A gray band, approximately 40 nm in thickness, is evident within the film between the tungsten metal and the porous alumina film. The interface between these differently contrasted film regions appears quite well-defined. Columns of material, generally similar in contrast to the band, about 125 nm in height, extend at intervals from the band outward into the pores in the alumina film. With reference to the interpretation of SEM data presented in previous works,[12,13] the band and columns represent regions containing tungsten oxide, revealed by its darker appearance comparatively to the residual tungsten layer. The observed contrast can be due to relatively lower yield of secondary electrons from the oxide-containing region because of its anodic oxidation.[12]

(24) Vrublevsky, I.; Parkoun, V.; Schreckenbach, J.; Goedel, W. A. *Appl. Surf. Sci.* **2006**, *252*, 5100.
(25) Zhou, X.; Thompson, G. E.; Skeldon, P. *Electrochim. Acta* **2008**, *53*, 5684.

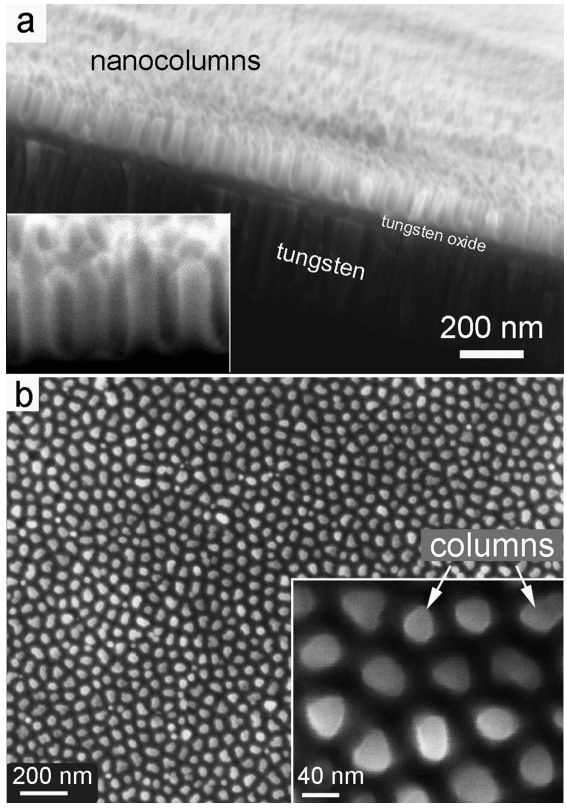

Figure 4. SEM images of (a) fracture section and (b) the surface of the Al/W/Ti/Si sample after anodizing followed by reanodizing as in Figure 2 and selective dissolution of the porous alumina film (alumina-free specimen).

Most of the columns have additional, arrow-like regions of material raised from the column tops and extending along the alumina pores, with the height from 20 to 50 nm (Figure 3d). These protrusions represent tungsten oxide because they extend from, and have similar contrast with, the column material: tungsten oxide developed by anodic oxidation of the tungsten layer.

To dissolve the alumina part of the film and examine merely the TO nanocolumns, selected specimens were immersed for about 20 min in a selective etchant (a mixture of phosphoric and chromic acids at 70−80 °C).[12] Then the specimens were rinsed in distilled water and dried in an air stream. The films thus prepared are further referred to as the alumina-free specimens. SEM micrographs taken of the alumina-free specimen are shown in Figure 4. Arrays of nanosized columns, about 125 nm in height, standing upright on the substrate are observed in Figure 4a. The residual tungsten is seen in the lower part of the micrograph, separated from the column array by a relatively uniform band, with a thickness of about 40 nm. Following the above interpretation, the band and columns represent regions containing TO, as it will be confirmed later. On the images of Figure 4b, the light areas are associated with the TO columns whereas the black regions surrounding the columns appear due to the greater scattering of the primary electron beam and secondary electrons generated from the bottom material, although it is TO as well. From the top-view images, the columns are regularly arranged, covering more than 30% of the specimen surface. An average diameter of the columns (the diameter of the equivalent circle) was estimated to be 40 nm, which

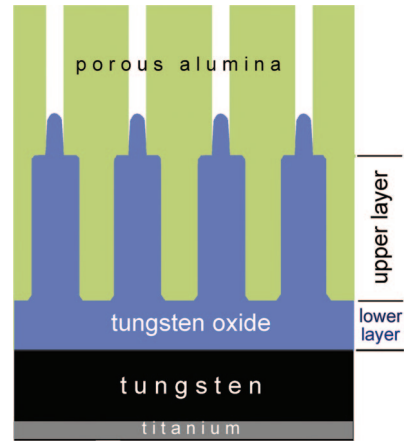

Figure 5. Schematic cross section of the Al/W/Ti layers anodized and reanodized as in Figure 2.

is more than 3 times the average pore size (12−15 nm) in the top alumina film. A schematic representation of the anodic film section with layered film composition is drawn in Figure 5. The columnar part of the film and the continuous TO layer formed under the columns are further referred to as the upper layer and the lower layer, respectively (Figure 5). The formation conditions and the measured film parameters are summarized in Table 1.

XPS and ToF-SIMS Results. The presence of C, W, O, Al, and Si was identified in the wide-scan survey spectra recorded on the alumina-free sample. Narrow-scan XPS spectra were recorded to analyze the core levels of elements identified in the survey spectrum (C 1s, O 1s, Al 2p, Si 2p, and doublet W $4f_{7/2}$ W $4f_{5/2}$). The measured spectra were fitted using mixed Gaussian−Lorentzian functions with a Shirley background subtraction. All binding energies were referenced to the C 1s at 285.0 eV generated by photoelectrons emitted from carbon atoms in C−H bonds. Depth profiling was performed tracking the above elements.

Figure 6a shows the W 4f core-level spectrum recorded on the alumina-free sample and the result of its analysis. To reproduce the spectrum, four doublet peaks and the Shirley background were combined. The highest-intensity doublet peak, labeled as digit 1, with binding energies of 35.5 eV (W $4f_{7/2}$) and 37.7 eV (W $4f_{5/2}$) is associated with photoelectrons emitted from W atoms with +6 oxidation state (W^{6+}), that is, stoichiometric WO_3.[26] The other doublets in the spectrum correspond to tungsten suboxides. The doublet found at 1.1 eV lower binding energy (labeled as 2) is generated by photoelectrons emitted from W atoms with +5 oxidation state (W^{5+}) in W_2O_5.[27] The doublet labeled as 3, whose components are located at binding energies of 33.1 eV (W $4f_{7/2}$) and 35.3 eV (W $4f_{5/2}$) is generated by photoelectrons emitted from W atoms with +4 oxidation state (W^{4+}) in WO_2.[28] The highest-energy doublet (labeled as 4), with components at 36.7 eV (W $4f_{7/2}$) and 38.9 eV (W $4f_{5/2}$), can be associated with surface defects in WO_3-cation

(26) Moulzolf, S. C.; Ding, S. A.; Lad, R. J. *Sens. Actuators, B* **2001**, *77*, 375.
(27) Charton, P.; Gengembre, L.; Armand, P. *J. Solid State Chem.* **2002**, *168*, 175.
(28) Shpak, A. P.; Korduban, A. M.; Medvedskij, M. M.; Kandyba, V. O. *J. Electron. Spectrosc. Related Phenom.* **2007**, *156−158*, 172.

Table 1. Geometrical Characteristics of Alumina and Tungsten Oxide Films Formed by Anodic Processing of the Al/W/Ti/Si Sample

alumina film				tungsten oxide film				
anodizing voltage (V)	average oxide cell diameter (nm)	average pore diameter (nm)	population density of pores/cells (cm^{-2})	reanodizing voltage (V)	average column diameter (nm)	height of columns + protrusions (nm)	thickness of lower layer (nm)	population density of columns (cm^{-2})
27	70	12	2.7×10^{10}	100	40	125 + 45	40	2.6×10^{10}

vacancies.[29] It should be noted that for the specimens with the columnlike surface morphology, where the surface area is much larger than in a flat anodic film, the contribution of surface defects may have an important consequence for quantitative interpretation of the XPS spectra recorded at excitation energy of 1486 eV.

Analysis of the Al 2p core-level spectrum recorded on the alumina-free sample surface (not shown here) revealed that the spectrum can be reproduced by a symmetrical peak with binding energy of 75.0 eV and a full width at half-maximum (fwhm) of 1.8 eV, which is related to 2p electrons emitted from aluminum atoms in alumina (Al_2O_3).[30] No peaks associated with metallic aluminum were found in the spectrum.

The structure of the oxygen O 1s core-level spectrum at the sample surface was very complex. It is known that free oxide surfaces are always hydrated, that is, contain water molecules and hydroxyl groups. Besides that, the outermost layer of organic carbon contamination includes oxygen-containing functional groups, C—O and O—C═O species; the contribution from these species was clearly seen in the C 1s surface spectrum, which will be discussed later. Figure 6b shows the O 1s core-level spectrum recorded after five sputter cycles; most of the contaminants have been removed from the sample, and the oxide film is not hydroxylated. Two singlets separated by 1.0 eV with binding energies of 530.7 and 531.7 eV are used to reproduce the spectrum in Figure 6b. During the next five sputter cycles (not shown), the O 1s peak shape and position remained invariable; however, the intensity ratio of the lower-energy peak to the higher-energy peak decreased. Both peaks were present in the spectrum until the columnar part of the film was sputtered away. From the analysis of O 1s and Al 2p spectra and with reference to the reported data,[28,31] the singlets composing the O 1s spectrum can be assigned to oxygen species O^{2-} in WO_3 (the lower intensity) and in Al_2O_3 (the higher intensity). The reduction of the 530.7 eV peak intensity may be caused by a preferential oxygen sputtering from the tungsten trioxide.

Three singlets centered at 285.0, 286.5, and 288.3 eV are used to reproduce the C 1s core-level spectrum recorded on the as-received alumina-free sample surface (Figure 6c). These peaks are generated by photoelectrons emitted from carbon atoms, respectively, in C—H (C—C), C—O, and O—C═O groups.[32] After the sixth sputter cycle, the C 1s spectrum intensity was too low for an accurate measurement. The analysis of the C 1s spectrum shows that the carbon atoms are present not only in the outermost layer of organic contamination but are also incorporated in the anodic film in the form of C—O species. This conclusion can be further supported by the results of previous work[12] in which arrays of tantala nanocolumns were prepared and analyzed by XPS and the carbon peak vanished after the first cleaning cycle.

SEM-image insets in Figure 7a show the effect of the Ar^+ ion bombardment on the specimen surface during the depth-profiling analysis. The sputter rate was 0.4 A s^{-1}; each sputter cycle lasted 15 s. From the left micrograph, after the 10th sputter cycle, the columns still stand on the substrate, and no preferential erosion of the material is observed from the direction of the ion beam, pointed out by the arrow. The columns thinned and shortened quite smoothly and evenly at the commencement of sputtering. However, as the ion bombardment proceeded, simultaneous etching of the film material between the columns increased. This phenomenon, accompanying by increasing preferential oxygen sputtering, leads to long profiles with uncertain interfaces and inevitable ambiguity in their interpretation, both effects enhanced by the change in the film morphology (the right inset). Therefore, to realistically connect the sputter time with the depth of oxide removed, only the beginning of depth profiles can be considered.

Figure 7a shows the XPS profiles for atomic concentrations of the main elements of interest in the alumina-free specimen. The concentration of carbon, being rather high after the first sputter-cleaning cycle (20%), remains appreciable up to the ninth sputter cycle. This means that the carbon-containing species are incorporated down to a depth of at least 10 nm. The concentration of Al (≈10%) does not change much throughout the film depth. As during the sputtering no peaks associated with metallic aluminum appeared in the Al 2p spectrum, the aluminum metal has been fully converted to aluminum oxide during the growth of anodic film. From the profiling behavior of the Al 2p peak, the alumina is not only present in the outermost film layer but it is also incorporated in the depth of the column material. Further, the ratio of oxygen to tungsten and aluminum atoms, [O:(W + Al)], is maximum in the beginning of sputtering (4.0), then gradually decreases to 2.7 when the carbon concentration goes to zero, and then further decreases to 2.0 at the 12th sputter cycle (≈10 nm depth), which corresponds to a mixture of the stoichiometric WO_3 and Al_2O_3. The existence of the oxygen-enriched region in the outer layer of the column material is due to the presence of nonstoichiometric oxygen (tungsten vacancies in the tungsten trioxide), bound water, and

(29) Nanba, T.; Ishikawa, M.; Sakai, Y.; Miura, Y. *Thin Solid Films* **2003**, *445*, 175.
(30) Wagner, C. D.; Moulder, J. F.; Davis, L. E.; Riggs, W. M. *Handbook of X-ray Photoelectron Spectroscopy*; Perkin-Elmer Corp.: New York, 1979.
(31) Hofmann, S. In *Practical Surface Analysis, Auger and X-ray Photoelectron Spectroscopy*; 2nd ed.; Briggs, D., Seah, M. P., Eds.; John Wiley & Sons: New York, 1992; Vol. 1, p 169.
(32) McCafferty, E.; Wightman, J. P. *Surf. Interface Anal.* **1998**, *26*, 549.

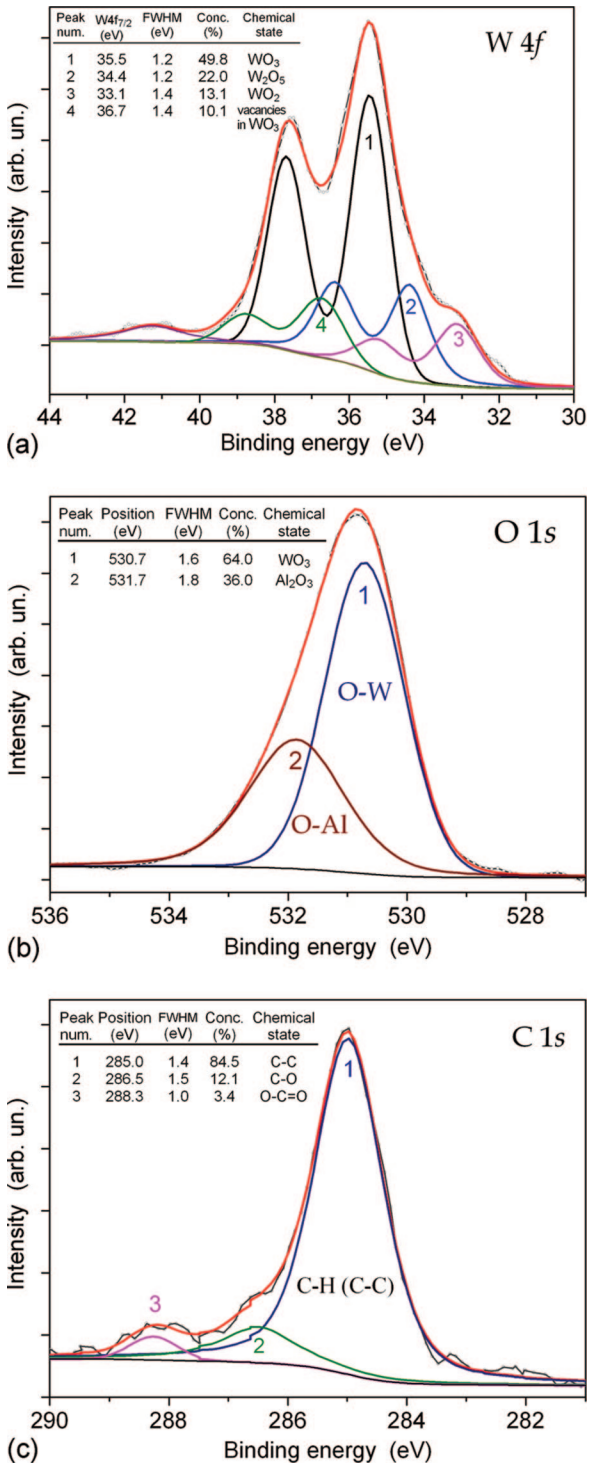

Figure 6. Experimental and fitted (a) W 4f, (b) O 1s, and (c) C 1s core-level spectra of the Al/W/Ti/Si sample after anodizing followed by reanodizing as in Figure 2 (alumina-free).

incorporated $C_2O_4^{2-}$ anions inherited from the alumina cell walls. The concentration of silicon is below 3% at the film surface and rapidly decreases to a negligible value during the first sputter cycles.

The distribution of low-concentration Si species was better revealed by the more sensitive ToF-SIMS. Both positive and negative ToF-SIMS spectra were obtained in the mass range up to $m/z < 200$ for the alumina-free specimen. Figure 7b shows the ToF-SIMS depth profiles of the following characteristic fragment ions from the specimen: SiO_2^- (m/z

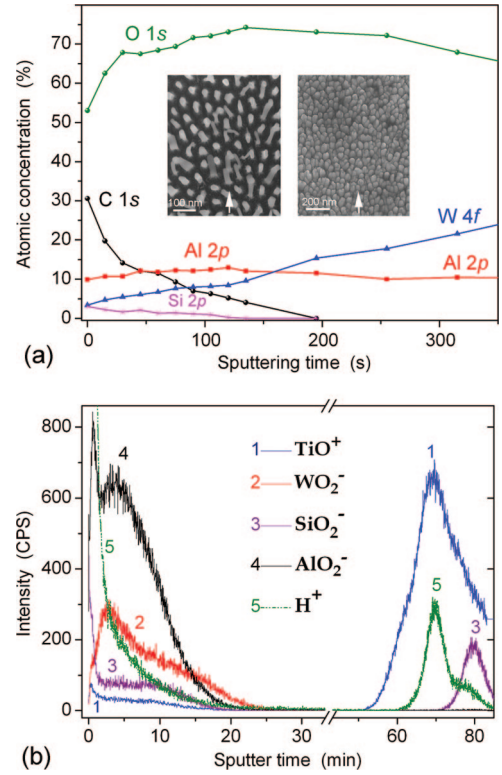

Figure 7. (a) XPS atomic concentrations profiles and (b) ToF-SIMS depth profiles for the Al/W/Ti/Si sample after anodizing followed by reanodizing as in Figure 2 (alumina free). The inset images in (a) show the film surface after the 10th sputter cycle (left) and at the end of the Ar^+ ion etch (right).

= 60), WO_2^- (184), AlO_2^- (59), TiO^+ (64), and H^+. The WO_2^- fragments originating from tungsten oxide and H^+ fragments are used as marker elements for distinguishing between the anodic film and the residual metallic (unoxidized) tungsten layer, in which the presence of the above components is unlikely. The SiO_2^- fragment is registered throughout the anodic film depth, and the intensity of the SiO_2^- line is substantially higher at the film surface. This implies that the silicon-containing species are incorporated in the film structure. Another interesting feature is the presence of oxidized Ti in the film composition. Although the concentration of Ti-containing species in the anodic film is below 1% (not detectable by XPS), these species are distributed throughout the entire film depth. Neither Si- nor Ti-containing fragments were found in the region of the ToF-SIMS spectra associated with the residual layer of tungsten metal (20−60 min of sputtering in Figure 7b). The oxidized Si and Ti may appear in the anodic film due to outward migration of Si^{4+} ions from the substrate and the Ti^{4+} ions from the titanium underlayer and their reaction with water at the electrolyte/film interface. Further detailed investigation involving preparation and EDX point analysis of ultrathin cross sections of the anodic films is needed to determine the location and relative concentrations of Al, Si, Ti, and O separately within the columns and in the lower film layer.[12] It seems paradoxical that silicon and titanium ions, which are generated deeply beneath the tungsten layer, migrate outward through the remaining metal layers and contribute to the anodic film growth. Further, unlike the case of Al/Ta anodizing,[12] there is not a trace of evidence for boron

impurities in the anodic TO film. This means that boron-containing anions have not been incorporated in the anodic film. An explanation for the behavior observed is given later in the discussion section. Finally, the existence of Al_2O_3 in the alumina-free film is obvious from the ToF-SIMS profiles. The intensity of the representative AlO_2^- line is apparently higher in the outermost film region, which is associated with a higher alumina concentration in the outer column material.

XRD Results. First, XRD analysis was carried out for the alumina-free specimen that was heated to designated temperatures in the range of 25−800 °C in a controlled nitrogen atmosphere. Then, after the specimen was allowed to cool back down to room temperature, X-ray diffractograms were run again at the same experimental conditions but in the presence of static air in the high-temperature chamber. As an example, Figure 8a shows the X-ray diffractogram of the specimen that was heated in nitrogen to 800 °C and then cooled back to room temperature. The XRD pattern contains (010), (103), ($\bar{1}$04), and (004) reflections from $WO_{2.72}$ polycrystalline monoclinic phase with *P*2/*m* symmetry (ICDD file no. 01-073-2177). The diffractograms run at relatively lower temperatures (not shown) revealed that the $WO_{2.72}$ phase did not form at temperatures below 700 °C. An important feature is a preferential growth of the $WO_{2.72}$ nanocrystallites in the ⟨103⟩ direction. The four more peaks (Figure 8a) are associated with the reflections from tungsten disilicide (WSi_2) with the body-centered tetragonal lattice (ICDD file no. 01-081-2168).

Figure 8b displays the diffractogram of the alumina-free specimen reheated to 800 °C in air and then cooled back to room temperature. In addition to the $WO_{2.72}$ and WSi_2 crystal phases, the XRD pattern contains (002) and (112) reflections from the polycrystalline monoclinic WO_3 phase with *Pc* symmetry (ICDD file no. 87-2386). Obviously, the formation of the stoichiometric WO_3 phase is due to the temperature-accelerated diffusion of oxygen from the diffractometer chamber. Notably, the WO_3 crystallites grow textured in the ⟨010⟩ direction. The monoclinic $WO_{2.72}$ phase, which remains in the film structure after annealing in air, retains the initial ⟨103⟩ texture. The WSi_2 phase remains stable during annealing in air regardless of the temperature value, as well as after the specimen was allowed to cool back down to room temperature. Likely, the formation of tungsten silicide is related to the presence of silicon-containing species in the reanodized anodic film and will be discussed later in this paper.

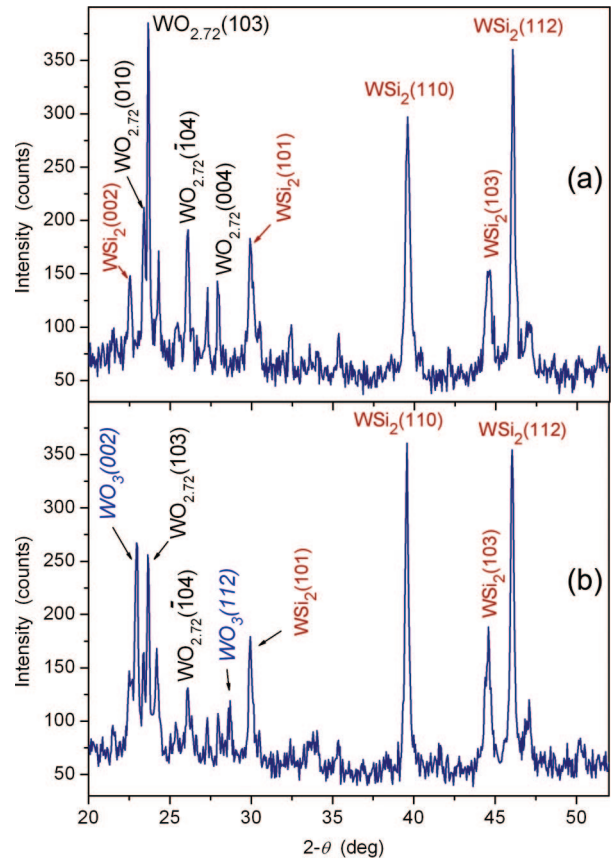

Figure 8. X-ray diffractograms of the Al/W/Ti/Si sample which had been sequentially anodized and reanodized as in Figure 2 (alumina-free): (a) after heating to 800 °C in nitrogen and then cooling back to room temperature, (b) after reheating to 800 °C in air and then cooling back to room temperature.

Discussion

Film Growth on Al/W/Ti Layers. Generally, barrier-type anodic films grown on tungsten at ambient temperatures are relatively thin, uniform, and usually amorphous and show little electron conduction.[33,34] During galvanostatic anodizing of tungsten, the anodic film thickens as the voltage rises with time in a linear manner until film growth is terminated by dielectric breakdown.[35] During anodizing of Al superimposed on W in barrier-type electrolytes, randomly occurring needlelike regions of tungsten oxide may randomly penetrate and irregularly mix with the upper alumina.[9] However, the ionic transport and anodic oxide growth become increasingly systematic when the Al/W couple is anodized in electrolytes for porous alumina formation: an array of nanosized TO bumps grows, as described in the previous sections. The main statements of the model of nucleation and growth of nanoscale oxide bumps during anodizing of tantalum, niobium, and titanium under the porous alumina film have been developed and justified in previous works.[10−13] Similar assumptions in the growth model are inherent for anodizing the Al/W couple. When the alumina barrier layer touches the tungsten, discrete TO regions begin to form at the Al_2O_3/W interface (Figure 9a), and the alumina continuously dissolves at the Al_2O_3/WO_3 interface due to dissociation of the Al−O bonds under the high field, similarly to the situation with anodizing the Al/Ta bilayer.[10] The O^{2-} ions released from the dissociating barrier layer participate in further oxidation of the tungsten while the released Al^{3+} ions migrate outward and are mostly expelled in the electrolyte.

In the Al/W/Ti trilayer sample, the Al layer is of nonuniform thickness, with variations up to roughly 50 nm. At sites where the deposited aluminum is thinnest, the film/

(33) Davies, J. A.; Domeij, B.; Pringle, J. P. S.; Brown, F. *J. Electrochem. Soc.* **1965**, *112*, 675.
(34) Shimizu, K.; Brown, G. M.; Habazaki, H.; Kobayashi, K.; Skeldon, P.; Thompson, G. E.; Wood, G. C. *Corros. Sci.* **1998**, *40*, 1229.
(35) Jeliazova, Y.; Kayser, M.; Mildner, B.; Hassel, A. W.; Diesing, D. *Thin Solid Films* **2006**, *500*, 330.

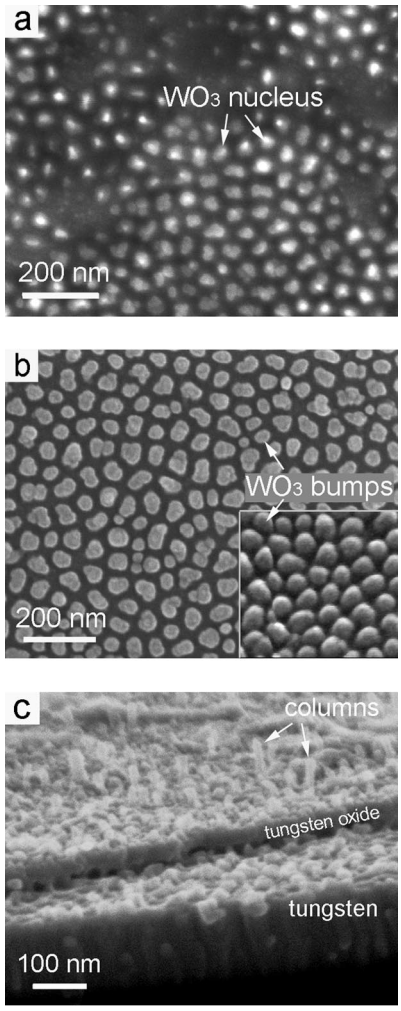

Figure 9. SEM images of (a, b) the surface and (c) a cross fracture of the Al/W/Ti/Si sample after anodizing followed by reanodizing to different stages (alumina-free): (a) the anodizing current begins to decay (part III in Figure 2a), (b) the current drops to leakage value (the end of part III in Figure 2a), and (c) the specimen is under-reanodized to 80 V without current decay.

metal interface reaches first the tungsten. At adjacent regions, there is still a residual amount of unoxidized aluminum. In the beginning, the current flows preferentially to the sites of tungsten oxidation, because the TO is of relatively lower ionic resistivity.[9] At these sites, the tungsten oxidizes with a large volume change, and nanosized TO regions are formed under the alumina cells and are forced into the alumina barrier layer (Figure 9a). The process continues until all the TO regions develop to their final bump-like shape, which is determined by the ionic resistances of the relevant oxides composing the film.[10] The lateral size of a TO bump is limited by the diameter of the corresponding alumina cell. The number of bumps may reach the number of pores in an ideal situation. As the amount of residual aluminum is reduced and further regions of tungsten metal are exposed, more TO bumps are generated, which tends to reduce the current to pre-existing bumps. The redistribution of current acts to slow the growth of bumps, as does also the widening of the oxide by displacement of alumina around a growing bump. An SEM image of the Al/W interface after the specimen was long anodized, until the current decreases to leakage value, is shown in Figure 9b.

During the reanodizing, the W layer is oxidized and new, columnlike oxide is continuously formed and directed into the pores via cross-migration of tungsten and oxygen ions. The situation when the TO tends to be confined to a narrow channel as it passes through the alumina pore competes with the phenomenon of widening of the oxide at the column bases. The column bases tend to group to create regions of increased dimensions until neighboring bases merge, since progress of oxidation should expose more tungsten at the metal/film interface. The exact relationship between the two concurrent directions of column growth, resulting in the formation of the upper and lower film layers, is determined by the degree of the following individual contributions: (i) the ratio of ionic resistivity of the oxide of the columns and the ionic resistivity of the alumina in the outer regions of the alumina cell walls; (ii) the transport number for tungsten species that migrate outward under the field; and (iii) the PBR value of tungsten oxide. Because a layer of residual tungsten metal remains after the reanodizing (Figures 3c,d and 4a), one may expect that the deep-lying Ti metal is excluded from the current passway.

As the voltage is raised, some columns grow first and retain a high current for sufficiently long times before the current redistribution limits their growth. A fracture of the specimen that was under-reanodized to about 80 V, without current decay yet, is shown in Figure 9c. Neither the lower nor upper film layer is yet of uniform thickness. But after the current decay period at 100 V, all of the columns become a uniform height and of a comparable diameter and the lower film layer gets a relatively uniform thickness. Obviously, this nearly ideal pore filling at the end of the reanodizing process is possible because the ionic resistivity of the oxide of the columns is rather comparable to the resistivity of the outer part of the alumina cell walls. This is unlike the case of anodic oxides grown on continuous W or Al layers in aqueous electrolytes, in which the difference in the ionic resistivities of the corresponding anodic oxides is more apparent.[9] Another difference is that the columns comprise an amount of tungsten suboxides, which exist in equilibrium with WO_3 and tungsten-deficient WO_3. With reference to early work by Arrora and Kelly[36] and most recent works by Blackman and co-workers,[18,19] the overall conclusion is that the present evidence for the nanostructured tungsten oxide having rare stoichiometry WO_2 and W_2O_5 is both experimentally and thermodynamically reasonable.

From Figure 3, the columns are apparently wider than the alumina pores and have well-defined boundaries with the adjacent alumina. The movement of the alumina to allow the column to develop could be due to the plasticity of the alumina film, as suggested by Iglesias-Rubianes and co-workers[9] for the case of the Al/W couple anodized in a barrier-type electrolyte. If this is the case, the growing anodic film should hold a high degree of deformation without cracking, which seems very unlikely even in amorphous anodic oxides. Apart from the above suggestions, in the present situation with the Al/W layers, the development of the columns, which is about 3 times wider than the alumina

(36) Arora, M. R.; Kelly, R. *J. Mater. Sci.* **1977**, *12*, 1673.

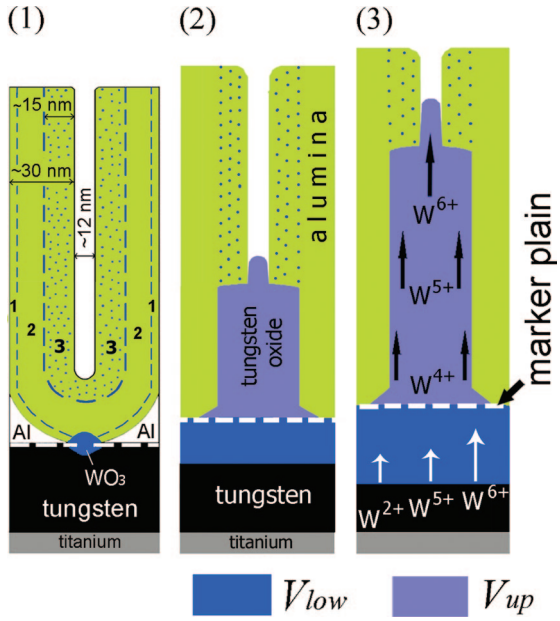

Figure 10. Schematic views of the Al/W/Ti layers showing the different stages of anodic processing: (1) the alumina barrier layer touches the W layer, (2) the reanodizing is half done (to 50 V), and (3) the reanodizing is completed (to 100 V). The numbered regions in (1) define the layers with different ion conduction. The arrows point out the migration of tungsten species.

pores, may be due to the penetration of the alumina cell walls by a displacement process, not just by the inherent plasticity in the oxides. Diagram (1) in Figure 10 shows a schematic section of the alumina cell with layers of different ion-conduction properties. The difference is noted between the outer part of the cell wall (layer 3), the intermediate layer 2, and the stoichiometric Al_2O_3 in the deepest region of the alumina barrier layer and cell walls (layer 1). A higher ionic conduction of layer 3 can be expected mainly due to the structural imperfections, like physical defects, cation vacancies, electrolyte species, and bound water included in the layer.[4,37,38] Nagayama and co-workers[39] explained the accelerated open-circuit dissolution behavior of the outer layer of the alumina cell walls by the greater degree of proton penetration into the vacancies in the oxide. On the basis of the SEM and XPS results, we assume that the situation with the Al/W layers is closely related to the conception developed in previous works on anodizing Al/Nb and Al/Ta[10,12,13] couples: during the growth of the TO nanocolumns most of the Al−O bonds in layer 3 (Figure 10) dissociate under the field as a result of the higher degree of structural imperfections and relatively lower resistivity of this layer. Experimental justification of the above mechanism may be obtained in future work by detecting the concentration of aluminum dissolved in the electrolytes by means of inductively coupled plasma optical emission spectrometry (ICP-OES).

Ionic Transport during Reanodizing. It is now commonly accepted that the anodic films on W and Al metals thicken due to migration of metal species toward the film surface and of oxygen species toward the metal[40] with new film material developing at the film/metal and electrolyte/film interfaces only. With reference to previous work,[12] it is expected that the cooperative ionic transport during the growth of the TO columns is more complex. In the usual case of tungsten anodizing, the transport number of tungsten species, that is, the ratio of ionic current carried by cations to the total ionic current, is determined from the ratio of the thickness of film material formed at the film surface and the total film thickness.[4,14] One of the objectives of the present study was to determine the effect of the presence of the porous-alumina top layer on transport numbers in the anodic TO for the given electrical and electrolytic conditions.

Transport numbers for cations and anions in anodic TO have been determined only for limited range of anodizing conditions near ambient temperature.[14,41,42] For example, for unpolished tungsten foil anodized at a constant current density of 0.1 mA cm^{-2} in 0.4 M KNO_3 + 0.04 M HNO_3 in water, transport numbers of metal and oxygen species were 0.3 and 0.7, respectively, using an ion-implanted xenon marker.[14] For tungsten anodizing at 1.0 mA cm^{-2}, a cation transport number of 0.37 was determined, suggesting an increase in the transport number with increased current density. In the present case of the regularly structured TO film generated in the alumina nanopores determination of the transport numbers during the reanodizing is based on the following statements: First, the tungsten metal under the porous alumina film is reanodized by sweeping up the voltage with a low and constant rate in the solution that chemically dissolves neither the alumina nor tungsten oxide. Second, the formation of new oxide occurs at both the electrolyte/TO interface (column tops) and the TO/metal interface (column bases) due to outward migration of tungsten ions and inward migration of oxygen ions through the growing TO together in the upper (columnar) and lower (compact) film layers. Further, the alumina-containing species are a relatively minor component of the film and can be neglected. The oxide formation at the electrolyte/column-top interface leads to filling the pores by the growing tungsten oxide. The oxide formation at the column bottoms/metal interface leads to bottoms expanding and merging in the continuous oxide layer beneath the alumina film [diagram (2), Figure 10]. As the interface between the lower and upper film layers is clearly identified (Figure 3d), this interface can be used as a "marker plane"[7] (Figure 10). Therefore, the transport number of oxygen ions t_O responsible for anodic oxide growth at the oxide/metal interface is defined as

$$t_o = \frac{V_{low}}{V_{tot}} = \frac{V_{low}}{V_{low} + V_{up}} \quad (1)$$

where V_{low} is the volume of new TO formed under the pores (the lower film layer); V_{up} is the volume of new TO formed within the pores (the upper film layer); and V_{tot} is the total volume of new TO formed (Figure 10). Using eq 1, t_O = 0.52 is estimated from the volumes of the corresponding oxide portions calculated from the measured film parameters

(37) Murphy, J. F.; Michelson, C. E. *J. Electrochem. Soc.* **1968**, *115*, 218.
(38) Nagayama, N.; Tamura, K.; Takahashi, H. *Corros. Sci.* **1970**, *10*, 617.
(39) Nagayama, M.; Tamura, K.; Takahashi, H. In *Proceedings of the International Congress on Metal Corrosion*; Sato, N., Ed.; National Association of Corrosion Engineers: Houston, TX, 1974; p 175.
(40) Pringle, J. P. S. *J. Electrochem. Soc.* **1974**, *121*, 865.
(41) Iglesias-Rubianes, L.; Skeldon, P.; Thompson, G. E.; Habazaki, H.; Shimizu, K. *Corros. Sci.* **2003**, *45*, 2905.
(42) Kim, D.-J.; Pyun, S.-I. *Electrochim. Acta* **1998**, *43*, 2341.

given in Table 1. Complementing the oxygen ions, the transport number of tungsten ions is 0.48. Thus, the measured t_O value is lower than that reported elsewhere for anodic films grown on uncovered tungsten at room temperature. Respectively, the measured transport number for the cation exceeds any of the reported values.[9,14] This discrepancy implies that the ionic transport in the nanostructured anodic TO is more complex than in a uniform WO_3 film grown on tungsten in a variety of electrolytes. The increased transport number for tungsten species can be explained by assuming that, in addition to W^{6+} ions, tungsten ions of lower oxidation states are generated at the oxide/metal interface under the given conditions. Considering the present XPS results and the findings of previous works on Al/Ta anodizing,[12,13] one can expect that W^{5+} and W^{4+} ions migrate in the outer layer of column material to form tungsten suboxides at the electrolyte/oxide interface (Figure 10). In this sense, the measured transport number is the composite value, that is, an average value of all migrating tungsten ions with different oxidation states.

The migration of suboxidized tungsten ions in the outer column material can be an explanation for the specific, arrow-like appearance of the column tops (see Figure 3d). In the middle part of the growing columns, that is, within the alumina pores, the growth of new oxide is associated with the prevailing migration of W^{6+} species, which results in the growth of tungsten trioxide (WO_3), having the biggest volume expansion. The outer portion of the column material is formed due to the migration of tungsten ions, with relatively lower oxidation states, which results in the formation of tungsten suboxides W_2O_5 and WO_2 and the outermost WO_3 with cation vacancies. The growth of these oxides is accompanied by relatively smaller volume expansion than that related to the stoichiometric WO_3. Thus, the PBR for the oxide grown within the volume of the pores is larger than that for the oxide formed beside the volume of the pores. Because the WO_3 grows preferentially within the alumina pores, the protrusions, which come out from the column tops (Figures 3d and 10), are mostly tungsten trioxide. Additionally or alternatively to the above explanation, the protrusions on the column tops may form due to the higher flux rate in the central zone than in the peripheral part of the columns because the ionic resistivity of the outer alumina cell region is higher than that of the tantalum pentoxide in the column center.

The presence of silicon-containing species in the column material can be reasonably explained as follows. During the reanodizing, silicon atoms at the Ti/Si interface get oxidized, and potentially mobile silicon ions, for example, Si^{4+}, begin to migrate outward, reaching eventually the electrolyte/column interface. Some of these mobile silicon ions are expelled to the electrolyte, but the others react with oxygen from the electrolyte and participate in the formation of stable solid-state oxides at the column tops within the alumina pores. The outward migration of Si^{4+} ions through the remaining titanium and tungsten layers can only be possible if the metallic films grew partly oxidized during the sputter deposition. The percentage and stoichiometry of oxide inclusions in an rf-magnetron-sputtered metal film is known to depend upon the residual oxygen pressure in the deposition chamber and the temperature of the substrate. In the present case, because an external heating was used to improve the adhesion of the tungsten layer, the substrate temperature of about 100 °C was estimated over the deposition process. Considering the residual oxygen pressure, it can be expected that the sputtered atoms partly oxidize in the argon-ion plasma in the vicinity of the substrate surface. The existence of the oxide inclusions in the sputtered W layer also explains the presence of Ti-containing species in the outer column material. Ti^{4+} ions that generate at the W/Ti interface during the voltage sweep migrate outward under the field and reach the electrolyte/film interface, where they meet O^{2-} anions and participate in the formation of new oxide in the alumina pores.

The formation of tungsten silicide can be the last step in a series of temperature-induced solid-state reactions: First, during the high-temperature annealing in nitrogen, tungsten ions in the less-stable tungsten suboxides (W_2O_5 and WO_2) are reduced to the metallic state due to the following disproportional reactions[36]

$$3WO_2 \rightarrow W + 2WO_3 \quad (2)$$

$$3W_2O_5 \rightarrow W + 5WO_3 \quad (3)$$

WSi_2 may also form due to the field-stimulated substitution reaction between the metallic tungsten and the silicon dioxide, which is present in the as-anodized film. Alternatively, the formation of tungsten silicide may result from a temperature-assisted interaction of Si with W, despite the titanium interlayer.[43] We will avoid making any further suggestions on this matter until more experimental and analytical work is completed.

Conclusions

Nanostructured tungsten-oxide film with self-organized columnlike surface morphology has been prepared by smart anodizing of Al/W/Ti metal layers deposited on a silicon wafer. Because of the remarkably systematic ionic transport during the film growth, the oxide nanocolumns (40 mn wide, up to 170 nm long, and 30 nm apart) had a complex chemical composition mainly comprising WO_3 with the surface defects, W_2O_5 and WO_2 suboxides, and Si-containing species. Crystallization of the amorphous anodic film was achieved at 700−800 °C with the formation of polycrystalline WO_3, $WO_{2.72}$, and WSi_2 phases, having remarkable crystal textures and postannealing stability.

The electrochemical method can be used for forming large-area nanostructured TO films with tailored morphologies relating to the wide-ranging, easy-controlled pore size and pore density in anodic alumina films generated in a variety of electrolytes.[4] Because of the enlarged, nanostructured surface and the presence of the polycrystalline tungsten suboxides and structural surface defects, the films prepared here are of interest as chemically and physically active layers for metal-oxide gas microsensors,[44] electrochromic devices, electro-optical coatings,[45] and hydrophilic or hydrophobic surfaces for biomedical applications.[46] From the technological viewpoint, the approach to fabricate nanostructured TO films is advantageous in that it allows easy integration with

(43) Weng, S.-L. *Phys. Rev. B* **1984**, *29*, 2363.
(44) Liao, L.; Lu, H. B.; Shuai, M.; Li, J. C.; Liu, Y. L.; Liu, C.; Shen, Z. X.; Yu, T. *Nanotechnology* **2008**, *19*, 175501.
(45) Lazarouk, S. K.; Leshok, A. A.; Borisenko, V. E.; Mazzoleni, C.; Pavesi, L. *Microelectron. Eng.* **2000**, *50*, 81.

existing semiconductor and thin-film technologies. Gas-sensing properties and technological compatibility of these TO films will be addressed in future work.

Acknowledgment. This work was funded in part by the Spanish Commission for Science and Technology under Project No. TEC2006-03671/MIC. A.M. acknowledges a mobility grant from the Autonomous Government of Catalonia and a Fellowship from the Max-Planck Society for Promotion of Science and International Scientific Exchange. We thank Dr. A.J. Smith of the Max-Planck-Institut für Eisenforschung (Düsseldorf, Germany) for his assistance with SEM observations.

CM801481Z

(46) Deval, J.; Umali, T. A.; Lan, E. H.; Dunn, B.; Ho, C.-M. *J. Micromech. Microeng.* **2004**, *14*, 91.